Spectral distribution and wave function of electrons emitted from a single-particle source in the quantum Hall regime

Battista, Francesca; Samuelsson, Peter

Published in:
Physical Review B (Condensed Matter and Materials Physics)

DOI:
10.1103/PhysRevB.85.075428

2012

Spectral distribution and wave function of electrons emitted from a single-particle source in the quantum Hall regime

F. Battista and P. Samuelsson
Division of Mathematical Physics, Lund University, Box 118, S-221 00 Lund, Sweden
(Received 19 December 2011; published 23 February 2012)

We investigate theoretically a scheme for spectroscopy of electrons emitted by an on-demand single-particle source. The total system, with an electron turnstile source and a single-level quantum dot spectrometer, is implemented with edge states in a conductor in the quantum Hall regime. Employing a Floquet scattering approach, the source and the spectrometer are analyzed within a single theoretical framework. The nonequilibrium distribution of the emitted electrons is analyzed via the direct current at the dot spectrometer. In the adiabatic and intermediate source frequency regimes, the distribution is found to be strongly peaked around the active resonant level of the turnstile. At high frequencies the distribution is split up into a set of fringes, resulting from the interplay of resonant transport through the turnstile and absorption or emission of individual Floquet quanta. For ideal source operation, with exactly one electron emitted per cycle, an expression for the single-electron wave function is derived.

DOI: 10.1103/PhysRevB.85.075428 PACS number(s): 72.10.−d, 73.23.−b, 73.43.−f

I. INTRODUCTION

The last decade has shown an increasing interest in transport in the integer quantum Hall regime, largely motivated by realizations of electric analogs of fundamental quantum optics experiments. Conductors in the quantum Hall regime provide the two key elements for electron optics experiments: Unidirectional edge states play the role of electronic waveguides[1,2] and quantum point contacts with controllable transparency act as tunable electronic beam splitters.[3–5] In their pioneering electron optics experiment, Ji *et al.*[6] investigated an electronic single-particle, or Mach Zehnder, interferometer.[7] This work was followed by a number of investigations, both experimental[8–13] and theoretical,[14–22] with the focus on the coherence and interaction properties of the interferometer. Recently, following the proposal in Ref. 23, a two-particle interferometer was realized experimentally by Neder *et al.*[24] The demonstration of two-particle interference provided a clear experimental connection[25] between edge-state transport and quantum-information processing.[26–34]

Another important aspect of edge-state transport, the high-frequency properties, was investigated in two key experiments. Gabelli *et al.*[35] analyzed the frequency-dependent admittance of a mesoscopic capacitor system. Good agreement was found with early theoretical predictions,[36] motivating additional investigations focusing on the effects of electron-electron interactions.[37–43] In the experiment by Feve *et al.*[44] a time-controlled single-particle source working at gigahertz frequencies was realized. It was demonstrated that a mesoscopic capacitor coupled to an edge state can serve as a time-periodic on-demand source, producing exactly one electron and one hole per cycle. The experiment was followed by a number of works investigating the accuracy and coherence of the source[45–51] and also proposing novel geometries with one or more on-demand sources as building blocks.[52–55] As an interesting example, a scheme for time-bin entanglement generation on demand was proposed in Ref. 56. Also other types of edge-state single-electron sources were investigated, both theoretically[57] and experimentally.[58,59] Of particular importance for the present work is the nonlocal electron-hole turnstile proposed by us,[57] which during ideal operation produces noiseless streams of electrons and holes along spatially separated edges.

An additional important tool for investigations of edge-state transport was demonstrated recently by Altimiras *et al.*[60] They developed a method for a spectroscopic analysis of the edge-state distribution, by weakly coupling a quantum dot with a single active level to the edge. In a series of works[60–62] the energy relaxation and the limitation of the electron-optics picture were investigated. Taken together, the achievements in the field to date makes it both experimentally accessible and fundamentally interesting to investigate spectral properties of electronic states emitted from single-particle sources. A successful experiment would open up for a detailed characterization of the state of the emitted particles. Moreover, for a source emitting electrons well above Fermi energy, the modification of the spectral properties of the particles propagating along the edge is a sensitive tool for investigating electronic interactions.[63–65]

In this work we perform a theoretical investigation of the electron spectral properties by analyzing a combined single-particle source-spectral detector system implemented with edge states in a multiterminal conductor; see Fig. 1. As the single-particle source we consider the turnstile of Ref. 57, although the analysis can readily be extended to other sources.[33,44,66,67] The distribution function of the electrons emitted by the source is investigated via the direct current flowing through the spectroscopic dot. We investigate the spectral distribution for the three physically distinct turnstile frequency regimes, adiabatic, intermediate, and high, identified in Ref. 57. It is found that in the adiabatic and intermediate regimes, the distribution is peaked around the energy of the active resonance of the turnstile. At the crossover to high frequencies the peak splits up, developing fringes due to the Floquet sidebands. At high frequencies a large number of features in the spectral distribution appears, related to resonant transport through higher lying turnstile levels. We discuss how these findings relate to earlier work on time-dependent

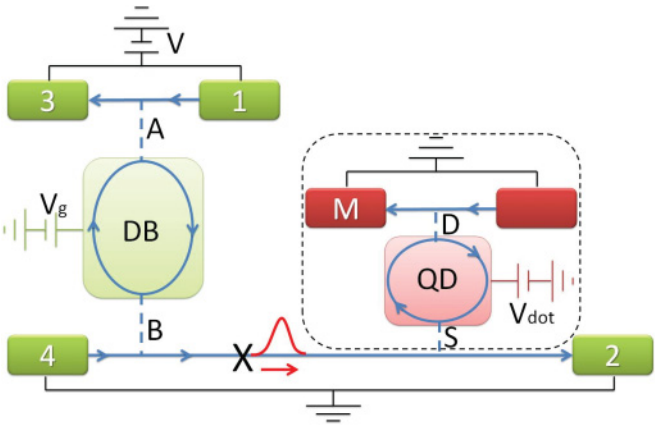

FIG. 1. (Color online) Schematic of the combined source-spectrometer system, implemented in a multiterminal conductor in the quantum Hall regime. Active spin-polarized edge states are shown with thick, blue lines, with arrows denoting the direction of propagation. The turnstile source (of Ref. 57) is shown to the left. A bias difference V is applied between terminals 1,3 and 2,4. Quantum point contacts A and B are driven by time periodic voltages. The double barrier (DB) region between A and B is capacitively coupled to a top gate (transparent green box), kept at a constant potential V_g. The emitted electron wave packet is shown schematically in red at position X. The spectrometer (of Ref. 60), shown inside the dashed box, consists of a quantum dot (QD), formed by static quantum point contacts S and D. The quantum dot, acting as an energy filter, has a single active level at energy $E_{\rm spec}$, controlled by the voltage $V_{\rm spec}$ applied to a top gate (red transparent box). Current is measured at terminal M.

transport in quantum-dot and double-barrier systems.[68–72] Moreover, we assess the robustness of our findings to, e.g., rectification effects and stray capacitive couplings. In addition, in the ideal turnstile regime we derive an expression for the wave function of single electrons emitted from the turnstile, giving complete information about the emitted state.

II. MODEL

The combined source-spectrometer system is implemented in a multiterminal conductor in the integer quantum Hall regime; see Fig. 1. Transport takes place along a single spin polarized edge channel. The single-particle source is the nonlocal electron-hole turnstile proposed in Ref. 57. Terminals 1 and 3 are biased at eV while terminals 2 and 4 are grounded. Electrons scatter between edges at the two quantum point contacts A and B, driven by time periodic voltages $V_A(t)$ and $V_B(t)$ with a period $\mathcal{T} = 2\pi/\omega$, π out of phase. The time-dependent transparencies of the contacts are $T_A(t)$ and $T_B(t)$. Throughout the paper, in the numerical analysis we model the contacts as saddle point constrictions[73,74] with sinusoidal driving potentials $V_A(t) = V_A^{\rm dc} - V_A^{\rm ac}\sin(\omega t)$ and $V_B(t) = V_B^{\rm dc} + V_B^{\rm ac}\sin(\omega t)$. However, the analytical results are valid for any contact transparencies and driving potentials giving a proper turnstile operation. The two quantum point contacts form a double barrier (DB) with a set of resonant levels in between. The energies of the resonant levels are taken to be time independent, controlled by the potential V_g applied to a top gate (see Fig. 1). The top gate has a large capacitance making charging effects negligible.[44]

In this paper we focus on the energy distribution of the electrons emitted toward terminal 2, while the properties of the emitted holes could instead be investigated by, e.g., changing the sign of the bias V at terminals 1 and 3. For the spectroscopy device we follow the edge channel spectroscopy experiment in Ref. 60 and consider a quantum dot weakly coupled to the output edge channel leading to terminal 2 (dashed box in Fig. 1). The quantum dot has only one active level at energy $E_{\rm spec}$, controlled by a top-gate voltage $V_{\rm spec}$. Electrons emitted by the turnstile can tunnel through the quantum dot to an edge channel fed from a grounded reservoir. The quantum dot acts as an energy filter and the energy distribution of the emitted particles can be extracted from the dc component of the current at lead M. We point out that the distance between the turnstile and the spectroscopy dot along the edge is smaller than the energy relaxation length.[61,62]

III. FLOQUET SCATTERING APPROACH

The energy distribution of the emitted particles is calculated within the Floquet scattering approach.[75–77] We first focus on the energy distribution $\bar{f}_{\rm out}(E)$ of the electrons emitted from the turnstile propagating toward the spectroscopy device, at a point denoted with X in Fig. 1. The relevant scattering matrices are the Floquet transmission matrices from lead 1 to X, $\tilde{t}_{X1}(E)$, and from 4 to X, $\tilde{t}_{X4}(E)$. The element $t_{X\beta}(E_m,E_n)$ of the matrix $\tilde{t}_{X\beta}$ is the amplitude for an electron incoming at energy $E_n = E + n\hbar\omega$ from terminal $\beta = 1,4$ to be emitted at energy E_m at X, picking up $m-n$ Floquet quanta $\hbar\omega$ when scattering at the time-dependent potentials. We have the matrices

$$\begin{aligned}\tilde{t}_{X1}(E) &= \tilde{t}_B\tilde{P}(E)[1-\tilde{r}_A\tilde{P}(E)\tilde{r}_B\tilde{P}(E)]^{-1}\tilde{t}_A,\\ \tilde{t}_{X4}(E) &= \tilde{r}_B + \tilde{t}_B[1-\tilde{P}(E)\tilde{r}_A\tilde{P}(E)\tilde{r}_B]^{-1}\\ &\quad\times\tilde{P}(E)\tilde{r}_A\tilde{P}(E)\tilde{t}_B.\end{aligned} \tag{1}$$

The matrix $\tilde{P}(E)$ is diagonal with elements $P(E_m,E_m) = \exp[i\phi(E_m)]$. The phase $\phi(E_m) = \phi_0 + \pi E_m/\Delta$ is acquired when the particle, at energy E_m, propagates a length L inside the DB, along the edge from A to B (or B to A) at drift velocity v_D. Here $\Delta = \pi\hbar v_D/L$ is the resonant level spacing in the DB and ϕ_0 is a constant phase, controlled by V_g. The Floquet matrices $\tilde{t}_A,\tilde{r}_A$, describing the scattering properties of quantum point contact A, are taken energy independent on the scale $\max\{kT,{\rm eV},N_{\rm max}\hbar\omega\}$, with T the temperature and $N_{\rm max}$ the total number of contributing sidebands. The matrix elements $t_{A,nm}$ of $\tilde{t}_A$ are then given by the Fourier transform of the time-dependent scattering amplitude $t_A(t) = i\sqrt{T_A(t)}$, i.e.,

$$t_{A,nm} = \frac{1}{\mathcal{T}}\int_0^{\mathcal{T}} e^{i(n-m)\omega t}t_A(t)dt, \tag{2}$$

and similarly for $r_A(t) = \sqrt{1-T_A(t)}$. The matrices $\tilde{t}_B,\tilde{r}_B$ describing the scattering properties of B are obtained in the same way.

The distribution function $\bar{f}_{\rm out}(E)$ is given by[76] the quantum statistical average of the occupation number of the outgoing edge at X. It can be written

$$\bar{f}_{\rm out}(E) = \sum_n \left[T^n_{X1}(E) f_V(E_n) + T^n_{X4}(E) f_0(E_n)\right], \quad (3)$$

where $T^n_{X\beta}(E) = |t_{X\beta}(E, E_n)|^2$ and $f_V(E)$ and $f_0(E)$ are the Fermi distribution functions of the biased and grounded reservoirs, respectively.

The experimental quantity of main interest is I_M, the direct, or time averaged, part of the current flowing into terminal M of the spectroscopy device (see Fig. 1). The spectroscopic quantum dot is weakly coupled to the edges via two quantum point contacts S and D with transparencies $T_S, T_D \ll 1$. Since there is only one active spin-polarized level in the dot, Coulomb effects are unimportant and the transport through the dot can be described as transmission through a Breit-Wigner resonance. A calculation, along the same line as for $\bar{f}_{\rm out}(E)$, of the direct current flowing into terminal M then gives

$$I_M = \frac{e}{h} \int T_{QD}(E) f_{\rm out}(E) dE, \quad (4)$$

where $T_{QD}(E) = \Gamma_S \Gamma_D / [([\Gamma_S + \Gamma_D]/2)^2 + (E - E_{\rm spec})^2]$ with $\Gamma_{S/D} = T_{S/D} \Delta_{\rm spec}/2\pi$ and $\Delta_{\rm spec}$ the level spacing of the dot. The distribution function $f_{\rm out}(E) = \bar{f}_{\rm out}(E) - f_0(E)$ is the difference between the distribution function of the electron emitted by the turnstile $\bar{f}_{\rm out}(E)$ and the distribution function $f_0(E)$ of a grounded reservoir. Importantly, to have a good resolution of the energy distribution, the width of the quantum dot resonance must be smaller than the energy scale δE on which $f_{\rm out}(E)$ changes, $\Gamma_S + \Gamma_D \ll \delta E$. In this limit we can effectively take $T_{QD}(E) \propto \delta(E - E_{\rm spec})$ and Eq. (4) turns into

$$I_M = \frac{e}{\hbar} \frac{\Gamma_S \Gamma_D}{\Gamma_S + \Gamma_D} f_{\rm out}(E_{\rm spec}). \quad (5)$$

Equation (5) shows explicitly that the direct current flowing to lead M is proportional to the energy distribution function $f_{\rm out}$ at energy $E_{\rm spec}$. The full energy dependence of the distribution can thus be reconstructed by continuously shifting $E_{\rm spec}$, achieved by tuning $V_{\rm spec}$.[60]

As will be clear from the discussion below, it is physically motivated to part the energy distribution function $f_{\rm out}(E)$ into two contributions: one due to the applied bias $f^{\rm bias}_{\rm out}(E)$,

$$f^{\rm bias}_{\rm out}(E) = \sum_n T^n_{X1}(E)[f_V(E_n) - f_0(E_n)], \quad (6)$$

and one coming from the pumping effect $f^{\rm pump}_{\rm out}(E)$,

$$f^{\rm pump}_{\rm out}(E) = \sum_n \left[T^n_{X1}(E) + T^n_{X4}(E)\right][f_0(E_n) - f_0(E)], \quad (7)$$

similar to the current partition in Ref. 57.

IV. FREQUENCY REGIMES

In the remaining part of the paper we focus on the distribution function $f_{\rm out}(E)$ and its parts $f^{\rm bias}_{\rm out}(E)$ and $f^{\rm pump}_{\rm out}(E)$ in different frequency regimes. Based on the findings in Ref. 57 we consider three qualitatively different regimes with adiabatic, intermediate, and high pumping frequencies highlighted in Fig. 2(a). We will for simplicity focus our investigation on the case with the applied voltage $eV = \Delta$ and one DB resonance within the bias window at energy $\epsilon_d = \Delta/2$. However the main results of the paper rely only on the fact that there is a single DB level well inside the bias window.

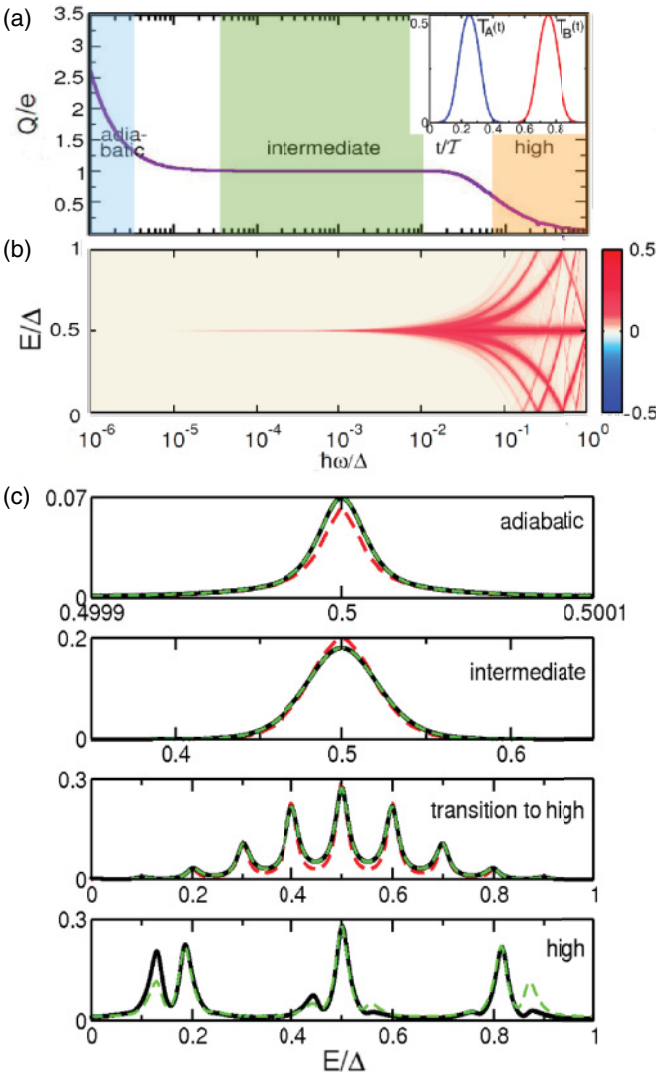

FIG. 2. (Color online) (a) Charge Q transferred by the turnstile per period, as a function of frequency with the three different regimes highlighted. Inset: Transparencies $T_A(t)$ and $T_B(t)$ for the driving scheme used in the numerical calculations throughout the paper. (b) Energy distribution $f_{\rm out}(E)$ as a function of pumping frequency and energy. (c) Energy distribution $f_{\rm out}(E)$ at $\hbar\omega = 10^{-6}\Delta$ (adiabatic frequency), $\hbar\omega = 10^{-2}\Delta$ (intermediate frequency), $\hbar\omega = 10^{-1}\Delta$ (transition to high frequency), and $\hbar\omega = 10^{-0.5}\Delta$ (high frequency) with (solid, thick black line) and without (dashed green line) pumping contribution. The red dashed lines show the analytical expressions obtained in the adiabatic [Eq. (11)], intermediate [Eq. (20)], and transition to high frequency regime [Eq. (22)]. In all the plots $kT \ll \Delta$.

A. Adiabatic-frequency regime

In the adiabatic regime the pumping period $\mathcal{T}$ is much longer than the time the particles spend inside the DB

region and many particles flow through the turnstile during one period.[57] Formally $N_{\max}\hbar\omega \ll \Delta\min_t[T_A(t)+T_B(t)]$; i.e., the total scattering matrix is energy independent on the scale $N_{\max}\hbar\omega$. The numerically calculated energy distribution function $f_{\rm out}(E)$ is plotted as a function of frequency in Fig. 2(b). We see that in the adiabatic regime the distribution is sharply peaked around the DB-region resonance energy.

To obtain a quantitative estimate of the shape of the distribution peak we note that to lowest order in frequency the Floquet scattering matrix elements defined in Eq. (1) are given by the Fourier coefficients of the frozen scattering amplitude[76] $t^0_{X\beta}(E,t)$ as

$$t_{X\beta}(E_n,E_m)=\frac{1}{\mathcal{T}}\int_0^{\mathcal{T}} e^{i(n-m)\omega t}t^0_{X\beta}(E,t)dt. \tag{8}$$

In our case the relevant frozen amplitudes are

$$\begin{aligned} t^0_{X1}(E,t)&=\frac{t_B(t)t_A(t)e^{i\phi(E)}}{1-r_A(t)r_B(t)e^{i2\phi(E)}},\\ t^0_{X4}(E,t)&=r_B(t)+\frac{r_A(t)t_B^2(t)e^{i2\phi(E)}}{1-r_A(t)r_B(t)e^{i2\phi(E)}}. \end{aligned} \tag{9}$$

Substituting Eq. (8) into Eqs. (6) and (7), and taking $f_V(E_n)-f_0(E_n)\simeq f_V(E)-f_0(E)$, we find that the bias contribution to the energy distribution is

$$f^{\rm bias,ad}_{\rm out}(E)=\frac{1}{\mathcal{T}}\int_0^{\mathcal{T}}\left|t^0_{X1}(E,t)\right|^2[f_V(E)-f_0(E)]dt. \tag{10}$$

The pump component is found to be a factor $\omega/\Delta\ll 1$ smaller than the bias contribution $f^{\rm bias,ad}_{\rm out}(E)$ and $f^{\rm pump,ad}_{\rm out}(E)$ is thus completely negligible; in Fig. 2(c) $f_{\rm out}(E)$ and $f^{\rm bias}_{\rm out}(E)$ fully overlap.

It is known[57] that the current flows through the DB region at times when the product $T_A(t)T_B(t)$ is maximal, i.e., around $t=n\mathcal{T}/2$. For those times $T_A(t),T_B(t)\ll 1$ and the electrons emitted by the turnstile will be distributed in energy according to the time average of a Breit-Wigner resonance at ϵ_d, with time-dependent width $\sim[T_A(t)+T_B(t)]\Delta$. Equation (10) then simplifies to

$$f^{\rm ad}_{\rm out}(E)\simeq\frac{1}{\mathcal{T}}\int_0^{\mathcal{T}}\frac{T_A(t)T_B(t)}{\left(\frac{T_A(t)+T_B(t)}{2}\right)^2+\left(\frac{2\pi(E-\epsilon_d)}{\Delta}\right)^2}dt, \tag{11}$$

where we used that $f_V(E)-f_0(E)\simeq 1$ for the energies of interest. From the plot in Fig. 2(c) we see that $f^{\rm ad}_{\rm out}(E)$ is in good agreement with the full numerics (the small-shape discrepancy is due to the frequency not being in the deep adiabatic regime).

B. Intermediate-frequency regime

In the adiabatic regime, for increasing pumping frequency the number of particles transversing the DB region during one period decreases as $1/\omega$. After a rapid transition into the nonadiabatic regime, there is[57] a wide pumping frequency interval $\Delta\min_t[T_A(t)+T_B(t)]/\hbar\ll\omega\ll\omega_A^{\max},\omega_B^{\max}$ with $\hbar\omega^{\max}_{A/B}=\Delta\min\{1,\int_0^{\mathcal{T}}(dt/\mathcal{T})\ln[1/R_{A/B}(t)]\}$, in which the turnstile works optimally and only one particle per period is pumped through the turnstile. As is clear from Figs. 2(b) and 2(c) the energy distribution of the electrons emitted in the optimal regime is still centered around ϵ_d, similar to the adiabatic regime, but it broadens and changes shape.

Again, to obtain a quantitative expression for the distribution function we first note that the pumping contribution $f^{\rm pump}_{\rm out}(E)$ is still a factor $\omega/\Delta\ll 1$ smaller than $f^{\rm bias}_{\rm out}(E)$. We can thus write

$$f_{\rm out}(E)\simeq f^{\rm bias}_{\rm out}(E)\simeq\sum_n T^n_{X1}(E)[f_V(E)-f_0(E)]. \tag{12}$$

For the energies of interest, around ϵ_d, $f_V(E)-f_0(E)\simeq 1$. To be able to treat arbitrary, nonadiabatic frequencies we introduce the dynamical scattering amplitude $t_{X1}(E,t)$, defined as[77]

$$t_{X1}(E,t)=\sum_n e^{in\omega t}t_{X1}(E,E_n), \tag{13}$$

for an electron injected from terminal 1 at time t to be emitted to X with energy E. We can then write Eq. (12) as

$$f_{\rm out}(E)=\frac{1}{\mathcal{T}}\int_0^{\mathcal{T}}|t_{X1}(E,t)|^2dt. \tag{14}$$

From Eqs. (1) and (13) we obtain (similar to Ref. 77)

$$t_{X1}(E,t)=t_A(t)\sum_{q=0}^{\infty}e^{i(2q+1)\phi(E)}L_q(t)t_B(t+[2q+1]\tau), \tag{15}$$

where $\tau=L/v_D$ and $L_q(t)=\prod_{p=1}^q r_A(t+2p\tau)r_B(t+[2p-1]\tau)$ for $q\geqslant 1$ and 1 for $q=0$. In the intermediate regime the time of flight τ through the DB region is much smaller than the pumping period, $\tau\ll\mathcal{T}$. We can then go from a discrete to a continuous description in time and write $t_{X1}(E,t)$ in Eq. (15) as

$$\begin{aligned} t_{X1}(E,t)\simeq -t_A(t)\frac{1}{2\tau}\int_0^{\infty}&\exp\left[i\frac{(E-\epsilon_d)}{\hbar}t'\right]t_B(t+t')\\ &\times\exp\left\{\frac{1}{2\tau}\int_0^{t'}\ln[r_A(t+t'')r_B(t+t'')]dt''\right\}dt'. \end{aligned} \tag{16}$$

In the optimal turnstile regime we can neglect[57] the times when both contacts A and B are simultaneously open and put $t_B(t)=0$ for $0<t<\mathcal{T}/2$ and $t_A(t)=0$ for $\mathcal{T}/2<t<\mathcal{T}$. Moreover, the current flows in and out of the DB region when the respective quantum point contacts are starting to open, i.e., $T_A(t),T_B(t)\ll 1$, and we can expand the logarithm in Eq. (16) to first order in $T_A(t),T_B(t)$. We can then write the quantity of interest

$$|t_{X1}(E,t)|^2=C_A(t)|c_B(E)|^2, \tag{17}$$

where we can identify

$$C_A(t)=T_A(t)\exp\left[-\frac{1}{2\tau}\int_t^{\mathcal{T}/2}T_A(\bar{t})\,d\bar{t}\right] \tag{18}$$

as the probability that an electron is injected at t and thereafter stays inside the DB region until $\mathcal{T}/2$. The energy-dependent

function

$$c_B(E) = \frac{1}{2\tau}\int_{\mathcal{T}/2}^{\infty} \exp\left[i\frac{(E-\epsilon_d)}{\hbar}t'\right] t_B(t') \times \exp\left[-\frac{1}{4\tau}\int_{\mathcal{T}/2}^{t'} T_B(t'')dt''\right]dt' \quad (19)$$

depends on the scattering properties of contact B only. The distribution function, Eq. (14), is then

$$f_{\rm out}(E) = \frac{\hbar\omega}{\Delta}|c_B(E)|^2 \quad (20)$$

since the time integral

$$\frac{1}{2\tau}\int_0^{\mathcal{T}/2} C_A(t)dt = 1 - \exp\left[-\frac{1}{2\tau}\int_0^{\mathcal{T}/2} T_A(\bar{t})d\bar{t}\right] \simeq 1 \quad (21)$$

gives[57] the probability that the DB region is charged at $\mathcal{T}/2$, unity in the optimal pumping regime.

The expression for $f_{\rm out}(E)$ in Eq. (20), together with Eq. (19), allows for a straightforward evaluation of the distribution function of the emitted electrons for any ideal turnstile driving scheme, once the time-dependent transparency $T_B(t)$ is known. As is clear from Fig. 2(c), the expression in Eq. (20) gives very good agreement with the full numerics.

1. Floquet fringes

At frequencies $\omega_{A/B}^{\max} < \omega < \Delta/\hbar$ the transferred charge starts to decrease, $Q < 1$ [see Fig. 2(a)], a consequence of incomplete charging and discharging of the DB region during the pumping cycle. In this frequency regime $f_{\rm out}^{\rm bias}(E)$ still determines the spectral distribution of the emitted charge; the pumping contribution $f_{\rm out}^{\rm pump}(E)$ can be neglected as the numerics show in Fig. 2(c).

From Fig. 2(b) we note that the resonance at ϵ_d starts to split up; i.e., $f_{\rm out}(E)$ develops a set of fringes at energies $\pm n\hbar\omega$ around ϵ_d, with $n = 0,1,2,3....$ The fringes are a manifestation of the integer number of Floquet quanta which the electrons gain or loose when transmitting through the DB region. Such manifestations of the interactions of transport electrons with an applied, time-dependent field have been intensively investigated in various forms in mesoscopic conductors; see, e.g., Refs. 68–71 for early works and Ref. 72 for a review. Typically the effect of the time-dependent field was investigated via transport quantities such as average current, differential conductance, or noise. Here we focus on the manifestation of the time-periodic field, i.e., the Floquet fringes, directly in the distribution function.

To obtain a quantitative description of the Floquet fringes we note that for well-separated fringes, only electrons which scatter resonantly through the DB contribute significantly to $f_{\rm out}(E)$. The resonant paths in energy-position space are shown in Fig. 3. One can divide the resonant process into three subsequent parts: (I) only electrons incident with an energy around $\epsilon_d \pm p\hbar\omega$, i.e., such that they can hit the resonance at ϵ_d by losing or gaining $p = 0,1,2,\ldots$ Floquet quanta $\hbar\omega$ at contact A, can enter the DB region; (II) inside the DB region electrons scatter elastically back and forth between A and B, i.e., without acquiring any quanta; (III) electrons emitted out through contact B pick up or lose n quanta and thereby

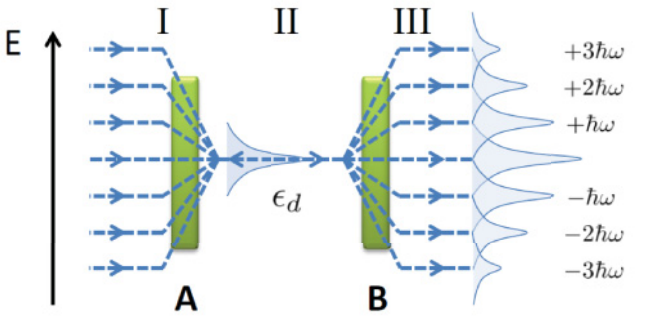

FIG. 3. (Color online) Schematic of the resonant paths in energy-position space, with three regions I, II, and III. In I electrons incident from terminal 1 pick up or lose a given number of Floquet quanta at contact A, to hit the resonance energy ϵ_d. In II, the DB region between A and B, the electrons scatter elastically back and forth between the contacts. In III the electrons acquire 0, ±1, ±2,... quanta when transmitting out through B.

contribute to the fringes at $\epsilon_d \pm n\hbar\omega$. Summing up all resonant paths we have from Eq. (6) and Eqs. (1), (2) that

$$f_{\rm out}(E) = \frac{\Delta}{2\pi}\sum_n \frac{\bar{\Gamma}_A|t_{B,0n}|^2}{([\bar{\Gamma}_A+\bar{\Gamma}_B]/2)^2 + (E_n-\epsilon_d)^2}, \quad (22)$$

where we use that $f_V(E_n) - f_0(E_n) \simeq 1$ and introduced $\bar{\Gamma}_{A/B} = (1/\mathcal{T})\int_0^{\mathcal{T}} dt\Gamma_{A/B}(t)$, the time average of the tunneling rate $\Gamma_{A/B}(t) = T_{A/B}(t)\Delta/2\pi$. The expression in Eq. (22) gives good agreement with the full numerics as shown in Fig. 2(c). From Eq. (22) we also see that fringes are given by a set of Lorentzians centered around $\epsilon_d + n\hbar\omega$, with a width $\bar{\Gamma}_A + \bar{\Gamma}_B$. The peak height of the fringes are proportional to $|t_{B,0n}|^2$, the modulus square of the Fourier components of the transmission amplitude through contact B. We point out that further numerical investigations (not presented) show that the occurrence of fringes of $f_{\rm out}(E)$ given by Eq. (22) is a generic feature for a turnstile with a single active DB level and hence not due to the specific parameters used in Fig. 2(b).

C. High-frequency regime

In the high-frequency regime the Floquet quantum $\hbar\omega$ becomes comparable to the DB-level spacing Δ. As a result the Floquet fringes from electrons scattering through DB resonances at energies $\epsilon_d + m\Delta$, $m = \pm1, \pm2,...$ start to contribute to $f_{\rm out}(E)$. As shown in Fig. 4, this leads to a dense pattern of fringes moving up and down in energy with increasing frequency $\omega > \Delta/\hbar$. In contrast to the adiabatic- and intermediate-frequency regimes, in the high-frequency regime the pumping contribution $f_{\rm out}^{\rm pump}(E)$ and the bias contribution $f_{\rm out}^{\rm bias}(E)$ are comparable [see Fig. 2(c)].

It is helpful for the physical understanding to discuss the properties of the two contributions separately. Starting with the bias contribution, we first note that $f_{\rm out}^{\rm bias}(E)$ is manifestly positive [see Eq. (6)], describing Floquet scattering of electrons injected from terminal 1, in the bias window. Moreover, with the resonance $\epsilon_d = \Delta/2$ in the middle of the bias window, the symmetry $f_{\rm out}^{\rm bias}(\epsilon_d + E) = f_{\rm out}^{\rm bias}(\epsilon_d - E)$ follows from Eq. (6) and is directly visible in Fig. 4(c). The energy of the fringes in $f_{\rm out}^{\rm bias}$ can be found by extending the

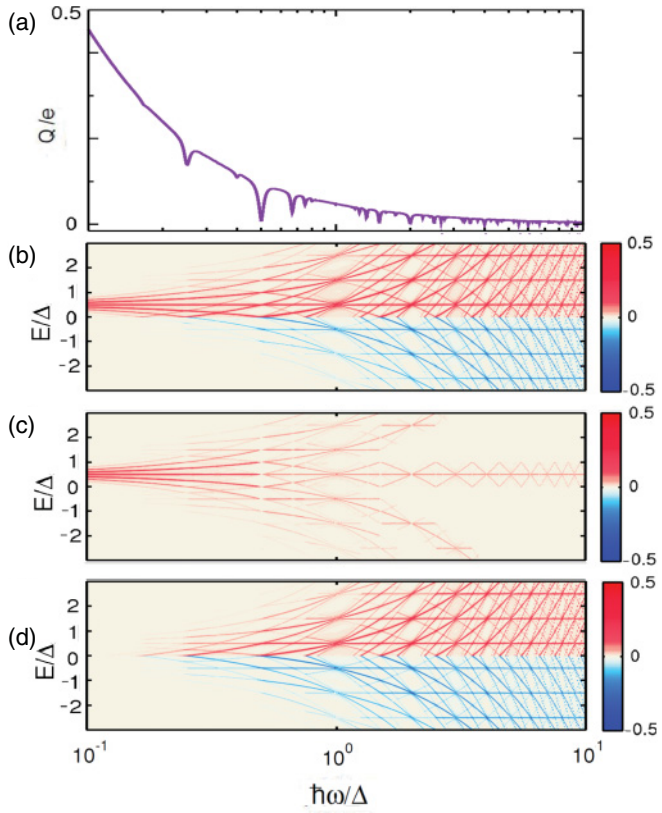

FIG. 4. (Color online) (a) High-frequency regime of the transferred charge Q per period, displaying dips at frequencies given by Eq. (23). (b)–(d) Energy distributions as functions of energy and drive frequency. The total distribution $f_{\rm out}(E)$ [in (b)], the bias contribution $f_{\rm out}^{\rm bias}$ [in (c)], and the pumping contribution $f_{\rm out}^{\rm pump}(E)$ [in (d)] are shown. In all the plots $T_A(t), T_B(t)$ as in Fig. 2 and $kT \ll \Delta$.

reasoning above: An incident electron which scatters through a DB resonance at $\epsilon_d + m\Delta$ and emits an additional $n = 0, \pm 1, \pm 2, \ldots$ quanta when transmitting out through contact B contributes to a fringe at an energy $E = \epsilon_{nm}$, given by

$$\epsilon_{nm} = \epsilon_d + m\Delta + n\hbar\omega. \tag{23}$$

Since the incident energy of the electron is restricted to the bias window, the bias component $f_{\rm out}^{\rm bias}$ will only show fringes at energies ϵ_{nm} fulfilling the additional requirement $\hbar\omega p \leqslant \epsilon_{nm} \leqslant \mathrm{eV} + \hbar\omega p$, with $p = 0, \pm 1, \pm 2, \ldots$. For $\hbar\omega > \mathrm{eV}$ this leads to bands of fringes, eV wide and separated by $\hbar\omega$, as is clearly seen in Fig. 4(c).

Turning to the pump contribution, $f_{\rm out}^{\rm pump}(E)$ describes the creation of electron-hole pairs out of the Fermi sea, due to the time-dependent potentials at the quantum point contacts A and B. The pump contribution has the symmetry $f_{\rm out}^{\rm pump}(E) = -f_{\rm out}^{\rm pump}(-E)$, also visible in Fig. 4(d). The origin of the fringes in $f_{\rm out}^{\rm pump}(E)$ is the same as for the bias part; however, since all electrons below Fermi energy in principle can contribute, in contrast to the bias part the fringes appear at all energies ϵ_{nm} given by Eq. (23).

Common for the fringes in $f_{\rm out}^{\rm bias}(E)$ and $f_{\rm out}^{\rm pump}(E)$ is that they typically are described as a set of superimposed Lorentzians of width $\bar{\Gamma}_A + \bar{\Gamma}_B$ in energy, just as described above for the intermediate-frequency regime [see Eq. (22)]. However, the height of the peaks depends in a more complicated way on through which resonances the particles have scattered as well as on the available energies for the injected electrons, giving a more complex peak structure. This is clear from the high-frequency regime panel in Fig. 2(c), where $f_{\rm out}^{\rm bias}(E)$ as well as the total distribution $f_{\rm out}(E)$, the experimentally accessible quantity, are shown.

1. Relation to transferred charge

It is interesting to relate the fringe properties of $f_{\rm out}(E)$ and its components to the transferred charge Q per cycle, discussed in Ref. 57 and plotted as a function of frequency for reference in Fig. 4(a). In the high-frequency regime, in addition to a slow, $\sim 1/\omega$, overall decrease with increasing frequency, the charge Q displays sharp dips at certain frequencies. In Ref. 57 these dips were explained by appealing to semiclassical electron paths through the turnstile leading to zero or small charge transfer. Here we first note that the charge Q is determined by $f_{\rm out}^{\rm bias}(E)$ only, since $Q = (e/h)\mathcal{T}\int f_{\rm out}(E)dE$ and $f_{\rm out}^{\rm pump}(E)$ is antisymmetric in energy around $E = 0$. By a direct comparison of the fringe structure of $f_{\rm out}^{\rm bias}(E)$ in Fig. 4(c) with the dips of Q in Fig. 4(a), we note that all dips occur for frequencies where different fringes cross, i.e., [from Eq. (23)] when $\epsilon_{nm} = \epsilon_{n'm'}$ with $n \neq n', m \neq m'$ giving the frequencies

$$\hbar\omega = \frac{m - m'}{n' - n}\Delta. \tag{24}$$

However, not all fringe crossings correspond to charge dips; e.g., while for $\hbar\omega = \Delta/2$ the dip in Q is large, for $\hbar\omega = \Delta$ there is no dip at all. The fringe structure around these two frequencies is illustrated in detail in Fig. 5(a).

To understand both the position and magnitude of the dips we note that crossing fringes correspond to a situation when an injected electron can take two (or more) different resonant paths in energy space and be emitted at the same energy E; see illustration in Fig. 5(b). As a consequence the two paths interfere, constructively or destructively, depending on the relative amplitudes for the two paths. To illustrate this which-energy-path interference[76] we consider two different paths where an electron injected at energy E_q scatters through a resonance at energy $E_n = \epsilon_d + m\Delta$ or $E_{n'} = \epsilon_d + m'\Delta$ and thereafter loses or gains n or n' quanta, respectively, and is emitted at energy E. The contribution to $f_{\rm out}^{\rm bias}(E)$ for this process is, then, similar to Eq. (22), exactly at resonance

$$4\frac{|t_{A,nq}t_{B,0n}e^{i\pi m\hbar\omega/\Delta} + t_{A,n'q}t_{B,0n'}e^{i\pi m'\hbar\omega/\Delta}|^2}{(\bar{\Gamma}_A + \bar{\Gamma}_B)^2}. \tag{25}$$

For the symmetric turnstile with π out of phase driving considered here we have $T_A(t) = T_B(t + \mathcal{T}/2)$ and consequently $t_{A,mn} = t_{B,mn}e^{i(m-n)\pi}$. The ratio of the interference, or coherent part and the incoherent part, is then given by

$$\frac{2t_{B,nq}t_{B,0n}t_{B,n'q}t_{B,0n'}\cos([m - m']\pi[1 + \hbar\omega/\Delta])}{|t_{B,nq}t_{B,0n}|^2 + |t_{B,n'q}t_{B,0n'}|^2}. \tag{26}$$

Noting that t_B,mn is purely imaginary, for e.g. $\hbar\omega = \Delta$ this ratio is maximal (the cosine term is 1 for all m,m'), i.e. constructive interference for all fringe crossings; see Fig. 5(a). For e.g. $\hbar\omega = \Delta/2$, the ratio summed over all resonances is minimal (the cosine term alternates between 0, -1 and

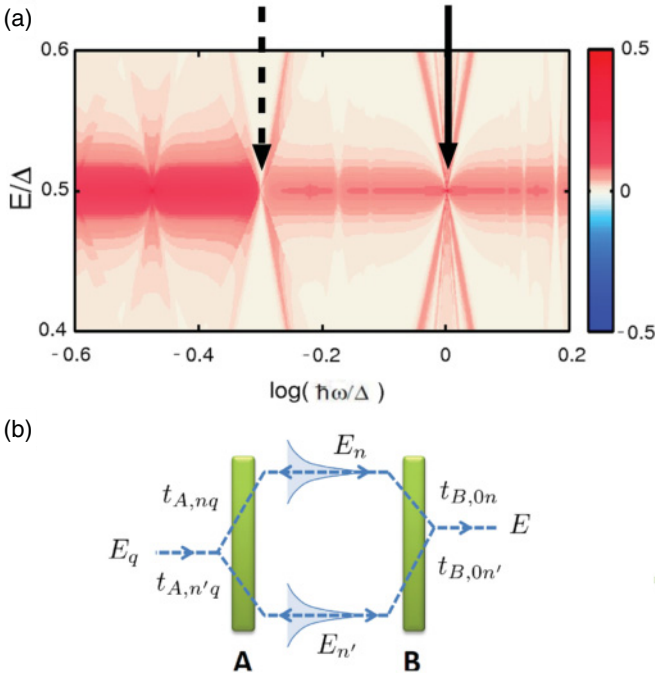

FIG. 5. (Color online) (a) Close-up of distribution function $f_{\rm out}^{\rm bias}(E)$ around frequencies $\hbar\omega \sim \Delta$, for energies around resonance $\epsilon_d = \Delta/2$. Strong suppression due to destructive interference is clear for $\hbar\omega = \Delta/2$ (dashed arrow) while no suppression occurs for $\hbar\omega = \Delta$ (full line arrow). (b) Schematic of two energy-position paths, going through two different resonances.

1 for different m,m'), i.e. destructive interference. For most crossings the ratio in Eq. (26) is somewhere in between, determined by the different probabilities for the individual paths $|t_{A,nq}t_{B,0n}|^2$ and the ratio ω/Δ. Taken together, the energy-path interference picture provides a quantum mechanical explanation for both the origin and the magnitude of the dips in the transferred charge Q, complementing and extending the semiclassical explanation given in Ref. 57.

V. WAVE FUNCTION OF EMITTED ELECTRONS, OPTIMAL TURNSTILE REGIME

Complete information about the state emitted by the turnstile is obtained from the full many-body wave function. The wave function is of key importance when investigating the possibilities for quantum-information processing with electrons in the quantum Hall regime. Of particular interest is the wave function for the electrons emitted in the optimal regime, with exactly one electron transferred per cycle. It would be desirable to derive the many-body wave function in the optimal regime along the lines of Ref. 66, where it was formally shown that the pump in the Fève *et al.*[44] experiment under ideal conditions creates a single electron (or hole) excitation on top of a filled Fermi sea. Here we however take a simpler path, which we nevertheless argue gives the same result in the optimal pumping regime.

During optimal operation the turnstile is completely charged and subsequently discharged, once each period.

In the second half of the pumping period, during the discharging, the quantum point contact A is closed and the

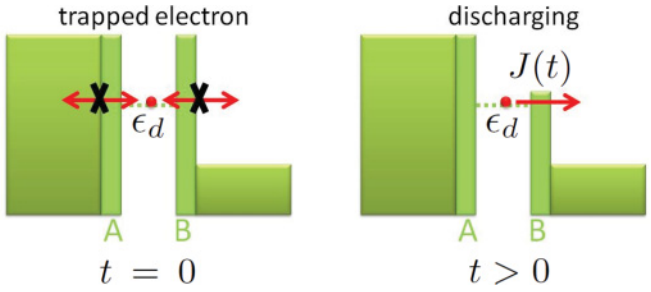

FIG. 6. (Color online) Sketch of the simplified model used to derive the single-particle wave function in the ideal regime. At $t = 0$ the electron is trapped between barriers, in a single level at energy $\epsilon_d = 0$. For $t > 0$ the electron can start to tunnel to the right lead. The time-dependent lead-level coupling is $J(t)$.

electron trapped in the DB can escape out through B (as sketched in Fig. 6). For $\hbar\omega \ll \Delta$ the escape takes place during times when $T_B(t) \ll 1$, i.e., soon after the opening of B at $t = \mathcal{T}/2$. Then only energies in a narrow interval $\sim T_B(t)\Delta$ around $\epsilon_d = \Delta/2$ are of importance. This allow us to neglect many-particle processes, related to excitations out of the filled Fermi sea, and consider a simplified single-particle model for the wave function of the emitted state. We thus describe the system during discharging with the Hamiltonian

$$H = \epsilon_d|d\rangle\langle d| + \sum_E E|E\rangle\langle E| + \sum_E J(t)[|d\rangle\langle E| + |E\rangle\langle d|], \tag{27}$$

where $|d\rangle$ denotes the DB level and $|E\rangle$ the chiral edge state of energy E, outside the DB region. The tunnel coupling $J(t)$ between the DB level and the edge is assumed to be energy independent. For notational convenience, in the model we count energies away from the dot resonance [$\epsilon_d = 0$ in Eq. (27)] and take the onset of the tunneling to occur at $t = 0$. We substitute the ansatz

$$|\psi(t)\rangle = c_d(t)|d\rangle + \sum_E c_E(t)|E\rangle \tag{28}$$

into the time-dependent Schrödinger equation $i\hbar d|\psi(t)\rangle/dt = H|\psi(t)\rangle$ and get the system of equations

$$i\hbar\dot{c}_d(t) = \sum_E J(t)c_E(t), \quad i\hbar\dot{c}_E(t) = Ec_E(t) + J(t)c_d(t), \tag{29}$$

subjected to the initial condition

$$c_d(t=0) = 1, \quad c_E(t=0) = 0. \tag{30}$$

Equations (29) with the boundary conditions in Eq. (30) can conveniently be solved by means of a Laplace transformation. For a continuum of states outside the DB, we find

$$c_d(t) = \exp\left[-\int_0^t \Gamma(\bar{t})d\bar{t}\right], \quad \Gamma(t) = \frac{\pi\nu}{\hbar}J^2(t), \tag{31}$$

where ν is the density of states of the edge. Using this expression for $c_d(t)$ we can solve the remaining equations in Eq. (29) and find

$$c_E(t) = \exp\left(\frac{-iEt}{\hbar}\right)\int_0^t \exp\left(\frac{iEt'}{\hbar}\right)\frac{J(t')}{i\hbar} \times \exp\left[-\int_0^{t'}\Gamma(\bar{t})\,d\bar{t}\right]dt'. \quad (32)$$

At times much longer than the emission time the DB region is completely discharged, $c_d(t) \to 0$, and the wave function $|\psi(t)\rangle$ only describes the emitted electron in the edge, a wave packet

$$|\psi(t)\rangle = \sqrt{\nu}\int c_E(t)|E\rangle dE. \quad (33)$$

To employ this result for composite systems, with, e.g., two or more turnstiles, it is desirable to construct the full many-body state corresponding to $|\psi(t)\rangle$. Reintroducing the Fermi sea, in second quantization we have

$$|\psi\rangle = \int_0^\infty \tilde{c}_E a_E^\dagger|0\rangle dE \quad (34)$$

in the Heisenberg picture. Here $a_E^\dagger$ creates an electron in the edge toward X in Fig. 1 at energy E; $|0\rangle$ is the filled Fermi sea. The coefficient $\tilde{c}_E = \sqrt{\nu}/(i\hbar)\int_0^t \exp[\frac{i(E-\epsilon_d)t'}{\hbar}]J(t')\exp[-\int_0^{t'}\Gamma(\bar{t})d\bar{t}]dt'$ reintroducing the turnstile level energy $\epsilon_d = \Delta/2$. From the wave function in Eq. (34) the average occupation number at energy E is given by $\langle\hat{n}(E)\rangle \equiv \langle a_E^\dagger a_E\rangle = |\tilde{c}_E|^2$.

To connect the wave function result with the Floquet approach above we first compare the probability for an electron to remain inside the DB after opening contact B, $|c_d|^2$, with the result of Ref. 57. We find, shifting the onset of the tunneling $\mathcal{T}/2$ in time in $J(t)$,

$$J(t) = \frac{1}{2\pi}\sqrt{\frac{\Delta T_B(t)}{\nu}}, \quad t \in [0,\mathcal{T}/2]. \quad (35)$$

We can then compare the distribution function in the optimal regime in Eq. (20) with the average occupation number from the wave function, giving

$$f_{\rm out}(E) = \hbar\omega\langle\hat{n}_E\rangle. \quad (36)$$

The factor $\hbar\omega$ in front of $\langle\hat{n}_E\rangle$ simply reflects the fact that while the wave function $|\psi\rangle$ describes a single electron emission, $f_{\rm out}(E)$ describes the periodic emission of single electrons, with a frequency ω. The relation in Eq. (36) provides evidence that the full many-body wave function for a single discharging event is given by Eq. (34). To obtain the wave function for several emitted electrons, well separated in time, one acts upon $|0\rangle$ with a product of wave packet operators $\int_0^\infty dE\tilde{c}_E a_E^\dagger$ with time translated tunnel couplings $J(t)$ [or equivalently $T_B(t)$], describing different emission times.

Importantly, the single-particle wave function for the emitted electron in Eq. (33) is valid for arbitrary tunnel coupling $J(t)$. However, we emphasize that special care must be taken when making the connection to the many-body wave function in Eq. (34). This is clearly illustrated by considering a steplike onset at $t = 0$; i.e., $J(t) = J\theta(t)$. This gives an amplitude

$$\tilde{c}_E = \sqrt{\frac{\hbar}{\pi}}\frac{\sqrt{\Gamma}}{i\hbar\Gamma + (E-\epsilon_d)}, \quad (37)$$

i.e., a Lorentzian wave packet centered around ϵ_d. The problem is that such a wave packet is not well confined inside the bias window $0 \leqslant E \leqslant \Delta$; the occupation decays as $\sim 1/E^2$ far away from resonance. As a consequence there is a nonnegligible probability to find the electron inside the filled Fermi sea or in a higher lying DB level, incompatible with the assumptions for the optimal pumping regime. This demonstrates that to make the connection between the wave functions in Eqs. (33) and (34), the time dependence of $J(t)$, and hence $T_B(t)$, has to be such that the resulting single-particle wave packet has no spectral weight outside the bias window.

VI. IMPERFECTIONS AND ROBUSTNESS

To assess the feasibility of our proposal it is important to investigate possible imperfections or deviations from the model which might become important in an experiment. In our opinion, the most important issue is the various effects of the capacitive coupling between the different components in the system, e.g., the gates, the reservoirs, and the electrons in the DB region.

First and foremost, we have so far in the paper assumed that the electrostatic potential of the DB is constant in time, due to a dominating capacitive coupling to the metallic top gate kept at a constant potential V_g (see Fig. 1). In an experiment, this might not be the case and it is interesting to investigate the effect of a capacitive coupling also to the gate at A and B, with applied time-dependent potentials $V_A(t)$ and $V_B(t)$. Second, a capacitive coupling between the gates at A and B and the electronic reservoirs 1 to 4 introduces a time-dependent component of the bias potential at the reservoirs. Such a time-dependent potential can lead to a rectification current[78] which can obscure the physical phenomena under investigation.[79,80]

Starting with the latter type of coupling, in our proposed turnstile, the rectification effects are typically not important in the adiabatic- and in the intermediate-frequency regimes. The reason for this is that a small ac potential at the reservoirs only leads to electron-hole excitations around energies 0 and eV of the grounded and biased reservoirs, respectively. These energies are far away from the resonance $\epsilon_d = \Delta/2$ where the net transport takes place. Hence, similar to the pumping contribution $f_{\rm out}^{\rm pump}(E)$, the rectification effects are negligible for frequencies $\omega \ll \Delta/\hbar$. At high frequencies $\hbar\omega \sim \Delta/e$ rectification effects might become important; their magnitude depends on the strength of the capacitive coupling between the gates at A and B and the reservoirs. A detailed investigation of these issues is however outside the scope of this paper.

For the first type of coupling, inducing a time-dependent potential in the DB, the situation is *a priori* less clear and we therefore investigate it in more detail. The isolated system, consisting of the spatially constant DB region capacitively coupled to the two quantum point contact gates A and B and the DB region top gate, can be represented in a simple circuit theory model as three capacitors of capacitances C_A, C_g, C_B put in parallel [see Fig. 7(a)]. Each of the capacitors is

subjected to a different voltage, $V_A(t), V_g, V_B(t)$, respectively, with $V_{A/B} = V^{\rm dc}_{A/B} \pm V^{\rm ac}_{A/B} \sin(\omega t)$ discussed above. The effective potential that the electron will experience in the DB region is $U(t) = U_0 + \delta U(t)$. For a typical driving scheme $V^{\rm ac}_A = V^{\rm ac}_B = V^{\rm ac}$ we find

$$\delta U(t) = \alpha V^{\rm ac} \sin(\omega t), \quad \alpha = \frac{C_B - C_A}{C_A + C_g + C_B}. \tag{38}$$

The constant part U_0 (determining ϕ_0 discussed above) is determined by the top-gate potential V_g. Equation (38) shows that in case of a dominant coupling with the gate, $C_g \gg C_A, C_B$, the asymmetry parameter $\alpha \ll 1$, and we can neglect $\delta U(t)$, as was done in the previous sections. Furthermore due to the π-shifted driving between A and B, the induced time-dependent potential is proportional to the difference $C_B - C_A$. For a symmetric capacitive coupling, $C_A = C_B$, we can thus also neglect $\delta U(t)$. To have an effect on $f_{\rm out}(E)$ the capacitive A,B-gate couplings thus have to be sizably asymmetric and of comparable strength to the DB top-gate coupling.

To calculate the effect of $\delta U(t)$ we note that a time-dependent, spatially constant potential in the DB can be formally taken into account[77] by modifying the Floquet matrix $\tilde{P}(E)$ in Eq. (1) to

$$P(E_n, E_m) = \frac{1}{\mathcal{T}} \int_0^{\mathcal{T}} e^{i(n-m)\omega t} dt \times \exp\left(i \left[\phi_0 + \frac{\pi E_n}{\Delta} - \frac{e}{\hbar} \int_t^{t+\tau} \delta U(t') dt' \right] \right), \tag{39}$$

which is then no longer diagonal. With the modified expression for the transmission matrices in Eq. (1) the spectral distribution $f_{\rm out}(E)$ can be calculated along the same line as above.

The effect of the induced time-dependent DB potential can be seen in the plot of $f_{\rm out}(E)$ in Fig. 7(c), where $e\alpha V^{\rm ac} = 0.1\Delta$. For the adiabatic (not shown) and intermediate frequencies the main effect is to shift the resonance in energy, away from ϵ_d, with the shift increasing for increasing frequency. While the size of the shift depends on ω and $|\alpha V^{\rm ac}|$, the direction, up or down in energy, is determined by the sign of $\alpha V^{\rm ac}$. The origin of the resonance shift can be understood by noting that the discharging of the DB region, at low and intermediate frequencies, takes place during a time interval much shorter than the period $\mathcal{T}$. As a consequence the electron leaving the DB region sees an essentially instantaneous potential $U(t)$. We can thus describe the shift by considering an effective, time-dependent level energy $\epsilon_d(t)$, depicted in Fig. 7(a). For the parameters in Fig. 7(c), the effective energy $\epsilon_d(t)$ is slightly below ϵ_d when the electron is emitted. The effective level picture is supported by the fact that the expressions for $f_{\rm out}(E)$ in the adiabatic- and intermediate-frequency regimes can be found by substituting $\epsilon_d \to \epsilon_d(t)$ in Eq. (11) and $\epsilon_d t' \to \int_0^{t'} \epsilon_d(t'')dt''$ in Eq. (19), respectively, where $\epsilon_d(t) = \epsilon_d + e\delta U(t)$. Importantly, the relatively small magnitude of the shift, given that $e\alpha V^{\rm ac} = 0.1\Delta$, results from the emission taking place soon after contact B starts to open, i.e., close to $t = \mathcal{T}/2$, where the time-dependent part $\delta U(t)$ is small. The lower the frequency, the closer to $t = \mathcal{T}/2$ the emission takes place. We also note that the fraction of the driving period during which the emission takes place becomes larger when the frequency increases, explaining the broadening of the resonance with increasing frequency seen in Fig. 7(c).

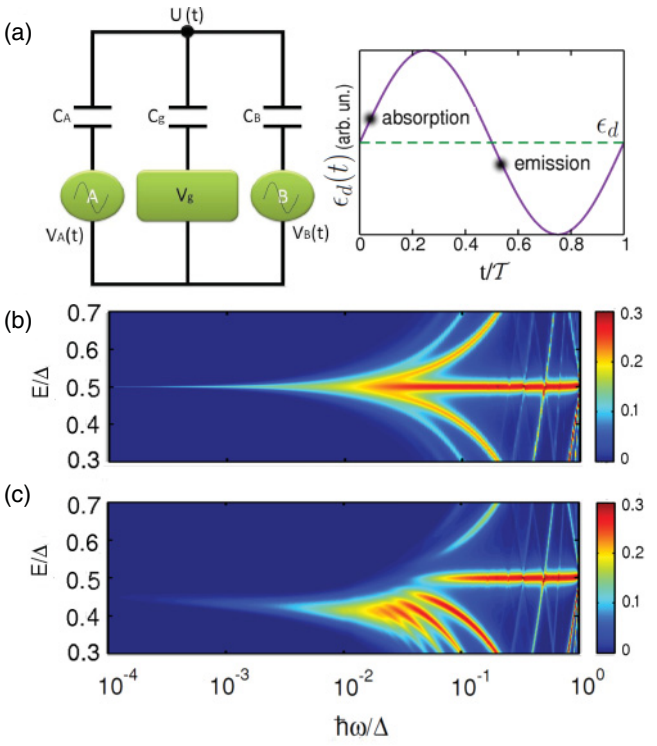

FIG. 7. (Color online) (a) Left: Circuit representation of the turnstile DB region capacitively coupled to quantum point contact gates A, B subjected to time-dependent bias $V_{A/B}(t)$ and a top gate kept at constant bias V_g. Right: Sketch of the oscillation of the effective, instantaneous resonant level energy $\epsilon_d(t)$. Times for absorption and emission of the electron from the DB region for typical system parameters are shown with black dots. (b) Energy distribution $f_{\rm out}(E)$ for asymmetry factor $e\alpha V^{\rm ac} = 0$ to compare with (c) $f_{\rm out}(E)$ for $e\alpha V^{\rm ac} = 0.1\Delta$ for a selected interval of E and ω.

The picture with emission from a time-dependent turnstile level at $\epsilon_d(t)$ breaks down for frequencies $\hbar\omega \sim \Delta$. In this high-frequency regime the main effect of a finite $\delta U(t)$ is to modify the magnitude and width of the individual Floquet fringes. In particular, an asymmetry between fringes corresponding to absorption and emission of Floquet quanta is clearly visible in Fig. 7(c). The details of this asymmetry can be analyzed in terms of which-energy-path arguments, similar to the above; this is however outside the scope of the present paper.

The main conclusion from this analysis is that the electron distribution, and hence the transferred charge, in the physically most interesting intermediate-frequency regime, is to a large extent unaffected by a time-dependent component of the potential inside the DB. Only when the time-dependent component becomes comparable to the level spacing Δ, of the order of meV in closely related experiments,[44,47] are the properties of the turnstile significantly modified. In our opinion, this investigation provides strong evidence for the robustness of the turnstile proposed in Ref. 57.

VII. CONCLUSIONS

We have performed a detailed theoretical investigation of the spectral properties of electrons emitted from an on-demand single-electron source. This was done by analyzing a combined single-particle source spectral detector system implemented with edge states in a multiterminal conductor. The single-particle source and spectrometer consisted of an electron turnstile and a single-level quantum dot, respectively. The distribution function of the electrons emitted by the source was investigated via the direct current flowing through the spectroscopic dot. We investigated the spectral distribution for three physically distinct frequency regimes: adiabatic, intermediate, and high. It was found that in the adiabatic and intermediate regimes, the distribution is narrowly peaked around the energy of the turnstile resonance. At the crossover to high frequencies the peak splits up, developing Floquet fringes. At high frequencies an analysis of the properties of the fringes and their relation to the charge transferred through the turnstile was examined, highlighting the role of which-energy-path interference. The robustness of the turnstile operation in the optimal regime was assessed, providing evidence for a large resilience to capacitive stray couplings and rectification effects. Moreover, in the ideal turnstile regime we derived an expression for the wave function of single electrons emitted from the turnstile and explained how to relate this to the full many-body wave function of the emitted particles. Our findings motivate an experimental investigation of the spectral distribution of electrons emitted from on-demand single-electron sources and put in prospect an observation of Floquet fringes, or sidebands, directly in the electron distribution.

ACKNOWLEDGMENTS

We acknowledge M. Moskalets, M. Büttiker, J. Splettstoesser, M. Albert, and C. Flindt for constructive comments on an earlier version of the manuscript. We also acknowledge support from the Swedish VR.

[1] B. I. Halperin, Phys. Rev. B **25**, 2185 (1982).
[2] M. Büttiker, Phys. Rev. B **38**, 9375 (1988).
[3] W. D. Oliver, J. Kim, R. C. Liu, and Y. Yamamoto, Science **284**, 299 (1999).
[4] M. Henny, S. Oberholzer, C. Strunk, T. Heinzel, K. Ensslin, M. Holland, and C. Schönenberger, Science **284**, 296 (1999).
[5] S. Oberholzer, M. Henny, C. Strunk, C. Schönenberger, T. Heinzel, K. Ensslin, and M. Holland, Physica E **6**, 314 (2000).
[6] Y. Ji, Y. Chung, D. Sprinzak, M. Heiblum, D. Mahalu, and H. Shtrikman, Nature (London) **422**, 415 (2003).
[7] G. Seelig and M. Büttiker, Phys. Rev. B **64**, 245313 (2001).
[8] I. Neder, M. Heiblum, Y. Levinson, D. Mahalu, and V. Umansky, Phys. Rev. Lett. **96**, 016804 (2006).
[9] L. V. Litvin, H.-P. Tranitz, W. Wegscheider, and C. Strunk, Phys. Rev. B **75**, 033315 (2007).
[10] P. Roulleau, F. Portier, D. C. Glattli, P. Roche, A. Cavanna, G. Faini, U. Gennser, and D. Mailly, Phys. Rev. Lett. **100**, 126802 (2008).
[11] E. Bieri, M. Weiss, O. Göktas, M. Hauser, C. Schönenberger, and S. Oberholzer, Phys. Rev. B **79**, 245324 (2009).
[12] P. Roulleau, F. Portier, P. Roche, A. Cavanna, G. Faini, U. Gennser, and D. Mailly, Phys. Rev. Lett. **102**, 236802 (2009).
[13] I. Neder, F. Marquardt, M. Heiblum, D. Mahalu, and V. Umansky, Nature Phys. **3**, 534 (2007).
[14] F. Marquardt and C. Bruder, Phys. Rev. Lett. **92**, 056805 (2004).
[15] V. S.-W. Chung, P. Samuelsson, and M. Büttiker, Phys. Rev. B **72**, 125320 (2005).
[16] H. Förster, S. Pilgram, and M. Büttiker, Phys. Rev. B **72**, 075301 (2005).
[17] S. Pilgram, P. Samuelsson, H. Förster, and M. Büttiker, Phys. Rev. Lett. **97**, 066801 (2006).
[18] E. V. Sukhorukov and V. V. Cheianov, Phys. Rev. Lett. **99**, 156801 (2007).
[19] J. T. Chalker, Y. Gefen, and M. Y. Veillette, Phys. Rev. B **76**, 085320 (2007).
[20] I. Neder and F. Marquardt, New. J. Phys. **9**, 112 (2007).
[21] I. P. Levkivskyi and E. V. Sukhorukov, Phys. Rev. B **78**, 045322 (2008).
[22] D. L. Kovrizhin and J. T. Chalker, Phys. Rev. B **81**, 155318 (2010).
[23] P. Samuelsson, E. V. Sukhorukov, and M. Büttiker, Phys. Rev. Lett. **92**, 026805 (2004).
[24] I. Neder, N. Ofek, Y. Chung, M. Heiblum, D. Mahalu, and V. Umansky, Nature (London) **448**, 333 (2007).
[25] P. Samuelsson, I. Neder, and M. Büttiker, Phys. Rev. Lett. **102**, 106804 (2009).
[26] C. W. J. Beenakker, C. Emary, M. Kindermann, and J. L. van Velsen, Phys. Rev. Lett. **91**, 147901 (2003).
[27] C. W. J. Beenakker and M. Kindermann, Phys. Rev. Lett. **92**, 056801 (2004).
[28] T. M. Stace, C. H. W. Barnes, and G. J. Milburn, Phys. Rev. Lett. **93**, 126804 (2004).
[29] P. Samuelsson and M. Büttiker, Phys. Rev. B **71**, 245317 (2005).
[30] C. W. J. Beenakker, M. Titov, and B. Trauzettel, Phys. Rev. Lett. **94**, 186804 (2005).
[31] P. Samuelsson and M. Büttiker, Phys. Rev. B **73**, 041305 (2006).
[32] V. Giovannetti, F. Taddei, D. Frustaglia, and R. Fazio, Phys. Rev. B **77**, 155320 (2008).
[33] Y. Sherkunov, J. Zhang, N. d'Ambrumenil, and B. Muzykantskii, Phys. Rev. B **80**, 041313 (2009).
[34] D. Frustaglia and A. Cabello, Phys. Rev. B **80**, 201312 (2009).
[35] J. Gabelli, G. Fève, J.-M. Berroir, B. Plaçais, A. Cavanna, B. Etienne, Y. Jin, and D. C. Glattli, Science **313**, 499 (2006).
[36] M. Büttiker, H. Thomas, and A. Prêtre, Phys. Lett. A **180**, 364 (1993).
[37] S. E. Nigg, R. López, and M. Büttiker, Phys. Rev. Lett. **97**, 206804 (2006).
[38] Ya. I. Rodionov, I. S. Burmistrov, and A. S. Ioselevich, Phys. Rev. B **80**, 035332 (2009).
[39] C. Mora and K. Le Hur, Nature Phys. **6**, 697 (2010).
[40] M. Filippone, K. Le Hur, and C. Mora, Phys. Rev. Lett. **107**, 176601 (2011).

[41] Y. Hamamoto, T. Jonckheere, T. Kato, and T. Martin, Phys. Rev. B **81**, 153305 (2010).
[42] M. Lee, R. López, M.-S. Choi, T. Jonckheere, and T. Martin, Phys. Rev. B **83**, 201304 (2011).
[43] O. Kashuba, H. Schoeller, and J. Splettstoesser, e-print arXiv:1109.6148.
[44] G. Fève, A. Mahé, J.-M. Berroir, T. Kontos, B. Plaçais, D. C. Glattli, A. Cavanna, B. Etienne, and Y. Jin, Science **316**, 1169 (2007).
[45] M. Moskalets, P. Samuelsson, and M. Büttiker, Phys. Rev. Lett. **100**, 086601 (2008).
[46] J. Keeling, A. V. Shytov, and L. S. Levitov, Phys. Rev. Lett. **101**, 196404 (2008).
[47] A. Mahé, F. D. Parmentier, E. Bocquillon, J.-M. Berroir, D. C. Glattli, T. Kontos, B. Plaçais, G. Fève, A. Cavanna, and Y. Jin, Phys. Rev. B **82**, 201309 (2010).
[48] M. Albert, C. Flindt, and M. Büttiker, Phys. Rev. B **82**, 041407 (2010).
[49] M. Albert, C. Flindt, and M. Büttiker, Phys. Rev. Lett. **107**, 086805 (2011).
[50] G. Haack, M. Moskalets, J. Splettstoesser, and M. Büttiker, Phys. Rev. B **84**, 081303 (2011).
[51] F. D. Parmentier, E. Bocquillon, J.-M. Berroir, D. C. Glattli, B. Plaçais, G. Fève, M. Albert, C. Flindt, and M. Büttiker, arXiv:1111.3136 (to be published).
[52] S. Ol'khovskaya, J. Splettstoesser, M. Moskalets, and M. Büttiker, Phys. Rev. Lett. **101**, 166802 (2008).
[53] J. Splettstoesser, S. Ol'khovskaya, M. Moskalets, and M. Büttiker, Phys. Rev. B **78**, 205110 (2008).
[54] C. Grenier, R. Hervé, E. Bocquillon, F. D. Parmentier, B. Plaçais, J.-M. Berroir, G. Fève, and P. Degiovanni, New J. Phys. **13**, 093007 (2011).
[55] S. Juergens, J. Splettstoesser, and M. Moskalets, Europhys. Lett. **96**, 37011 (2011).
[56] J. Splettstoesser, M. Moskalets, and M. Büttiker, Phys. Rev. Lett. **103**, 076804 (2009).
[57] F. Battista and P. Samuelsson, Phys. Rev. B **83**, 125324 (2011).
[58] C. Leicht, P. Mirovsky, B. Kaestner, F. Hohls, V. Kashcheyevs, E. V. Kurganova, U. Zeitler, T. Weimann, K. Pierz, and H. W. Schumacher, Semicond. Sci. Technol. **26**, 055010 (2011).
[59] F. Hohls, A. C. Welker, C. Leicht, L. Fricke, B. Kaestner, P. Mirovsky, A. Müller, K. Pierz, U. Siegner, and H. W. Schumacher, arXiv:1103.1746 (to be published).
[60] C. Altimiras, H. le Sueur, U. Gennser, A. Cavanna, D. Mailly, and F. Pierre, Nature Phys. **6**, 34 (2009).
[61] H. le Sueur, C. Altimiras, U. Gennser, A. Cavanna, D. Mailly, and F. Pierre, Phys. Rev. Lett. **105**, 056803 (2010).
[62] C. Altimiras, H. le Sueur, U. Gennser, A. Cavanna, D. Mailly, and F. Pierre, Phys. Rev. Lett. **105**, 226804 (2010).
[63] C. Neuenhahn and F. Marquardt, Phys. Rev. Lett. **102**, 046806 (2009).
[64] P. Degiovanni, C. Grenier, and G. Fève, Phys. Rev. B **80**, 241307 (2009).
[65] A. M. Lunde, S. E. Nigg, and M. Buttiker, Phys. Rev. B **81**, 041311(R) (2010).
[66] J. Keeling, I. Klich, and L. S. Levitov, Phys. Rev. Lett. **97**, 116403 (2006).
[67] M. Vanević, Yu. V. Nazarov, and W. Belzig, Phys. Rev. Lett. **99**, 076601 (2007).
[68] C. Bruder and H. Schoeller, Phys. Rev. Lett. **72**, 1076 (1994).
[69] L. P. Kouwenhoven, S. Jauhar, J. Orenstein, P. L. McEuen, Y. Nagamune, J. Motohisa, and H. Sakaki, Phys. Rev. Lett. **73**, 3443 (1994).
[70] T. H. Oosterkamp, L. P. Kouwenhoven, A. E. A. Koolen, N. C. van der Vaart, and C. J. P. M. Harmans, Phys. Rev. Lett. **78**, 1536 (1997).
[71] M. H. Pedersen and M. Büttiker, Phys. Rev. B **58**, 12993 (1998).
[72] G. Platero and R. Aguado, Phys. Rep. **336**, 1 (2000).
[73] H. A. Fertig and B. I. Halperin, Phys. Rev. B **36**, 7969 (1987).
[74] M. Büttiker, Phys. Rev. B **41**, 7906 (1990).
[75] M. Büttiker, Phys. Rev. B **46**, 12485 (1992).
[76] M. Moskalets and M. Büttiker, Phys. Rev. B **66**, 205320 (2002).
[77] M. Moskalets and M. Büttiker, Phys. Rev. B **78**, 035301 (2008).
[78] M. Büttiker, J. Phys. Condens. Matter **5**, 9361 (1993).
[79] M. Switkes, C. M. Marcus, K. Campman, and A. C. Gossard, Science **283**, 1905 (1999).
[80] P. W. Brouwer, Phys. Rev. B **63**, 121303 (2001).